TECHNICAL REPORT

In Situ Ion Irradiation to add Irradiation Assisted Grain Growth to the Marmot Tool

Arthur Motta - Pennsylvania State University - atm2@psu.edu

Most studies of grain growth in UO_2 are based on thermally driven processes at elevated temperatures. However, studies have shown that grain growth can occur even at cryogenic temperatures by ballistic processes. Such irradiation induced grain growth in UO_2 has yet to be studied. Advanced *in situ* Kr ion irradiation and Transmission Electron Microscopy (TEM) were systematically performed on nanocrystalline UO_2 thin films at temperatures ranging from 50 K to 1073 K; grain growth was observed at all temperatures. A combination of manual and machine learning techniques was used to measure and plot grain-size evolution against irradiation fluence at various irradiation temperatures. Data was fitted using classical grain growth and thermal spike models. The impact of irradiation on grain growth was also implemented in MARMOT.

Introduction

In the Nuclear Energy Advanced Modeling and Simulation (NEAMS) program, the MARMOT mesoscale fuel performance tool is used to inform the development of mechanistic materials models for the BISON fuel performance tool. The grain size of the fuel has a large impact on its performance, directly impacting heat conduction, fission gas release, creep, and fracture. Thus, atomistic and mesoscale MARMOT simulations have been used to investigate grain boundary migration and grain growth in UO_2 [1–2]. The mechanism for steady state thermal grain growth is the migration of individual grain boundaries to reduce the overall energy of the system, such that concave boundaries recede and convex boundaries advance. This results in the growth of some grains at the expense of the shrinkage and disappearance of other grains. In addition to thermal mechanisms, grain growth

has also been observed due to irradiation in both experiment [3] and simulation [4]. Grain growth resulting from irradiation is usually found to occur at a higher rate than thermal growth at intermediate temperatures. The motion of grain boundaries and growth of grains is commonly attributed to the thermal spikes that occur during the irradiation damage process. These "high temperature" spikes cause many atomic jumps. When a thermal spike overlaps one or more grain boundaries, a bias in atomic transport across the grain boundary caused by its curvature results in grain boundary migration and grain growth. The current grain growth model in MARMOT only considers grain growth kinetics of fresh, unirradiated fuel. Thus, it may be missing a crucial mechanism that could significantly hurt the accuracy of its predictions. The objectives of this project are twofold. First, the effects of irradiation on grain growth of UO_2 was experimentally investigated under various conditions and as a function of grain size. The impacts of isothermal annealing temperature and irradiation on grain growth kinetics were quantified in thin film UO_2 TEM samples using *in situ* techniques. Second, using the data obtained, the capabilities of the MARMOT tool have been expanded to account for the effects of irradiation on grain growth. The experimental data is being used to validate simulations run using MARMOT. Once complete, the expanded MARMOT capabilities will be used to assess the effects of irradiation on grain growth in light water reactor fuel pellets.

Fuel performance models must consider the effects of irradiation on the UO_2 grain growth.

Project Hypothesis

In the NEAMS program, the MARMOT code is used to inform the development of models for the BISON fuel performance tool. The fuel's grain size has a large impact on its performance. However, the current grain growth model in MARMOT only considers grain growth kinetics of fresh, unirradiated fuel. This work is to experimentally study irradiation effects on grain growth in UO_2 and implement these effects into MARMOT. This work is being performed using coincident and synergistic efforts of experiment and simulation. *In situ* TEM experiments were performed at the Intermediate Voltage Electron Microscopy (IVEM) Nuclear Science User Facilities (NSUF) partner facility at Argonne National Laboratory to study grain growth in both isothermal annealing and ion irradiation conditions.

Experimental or Technical Approach

The UO_2 samples were synthesized by pulsed laser deposition at Los Alamos National Laboratory. About 30 to 50 nm thick UO_2 thin films were deposited on SiN wafers, which contained an electron transparent window at the center. The samples were irradiated with 1 MeV Kr ions at the IVEM at temperatures ranging from 50 K to 1073 K. The ion dose rate of 6.25 x 10^{12} ions/cm^2/s corresponds to a total of over 10^{15} ions/cm^2 for the irradiation times used. Isothermal annealing experiments without irradiation were also conducted using the same TEM sample holder. The samples were characterized by systematically taking bright-field and dark-field images during irradiation as well as diffraction patterns. The quantified results on grain diameters at all temperatures and all fluences have been analyzed by using a manual and a machine learning method. The machine learning method utilized a U-Net architecture, which has a unique U-shaped architecture with a contracting path to extract image context and a symmetric expansive path to propagate context information to higher resolution layers [5]. An NVIDIA Tesla P100 GPU was used to train the model to 200 epochs with L2 Regularization. The training was terminated when the validation loss became stable. The total training time was about 6 hours.

The impact of irradiation was added to the existing UO_2 grain growth model in MARMOT [1, 2] by coupling it with a model of heat conduction in UO_2. Thermal spikes were added to the system by explicitly representing heat generation in the heat equation:

$$\rho C_P \frac{\partial T}{\partial t} = \nabla(k\nabla T) + \dot{q},$$

where $\partial T/\partial t$ is the rate of change of the temperature field T, k is the thermal conductivity, $\dot{q}$ is the volumetric heat generation term, ρ is the density, and C_p is the specific heat capacity. The heat generation term varied in time and space to account for the thermal spikes. When and where a thermal spike occurred in the domain was determined randomly. The spikes were defined by the magnitude of the heat source during a spike, the average rate at which the spikes occur in units of spikes per second per unit volume (a function of the fluence), the radius of the area over which

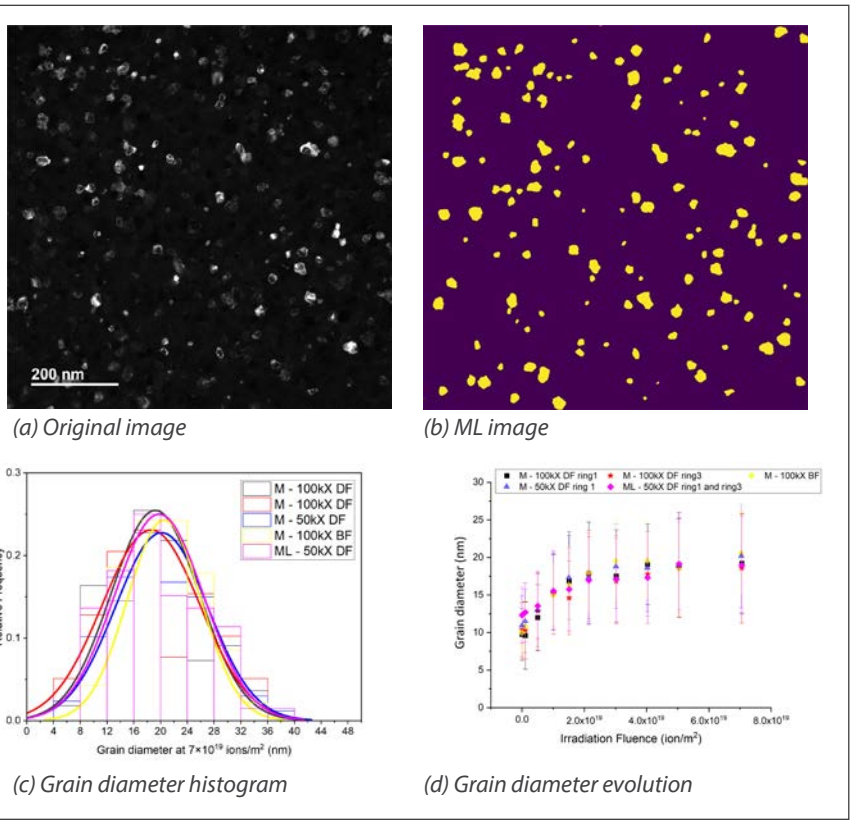

(a) Original image (b) ML image

(c) Grain diameter histogram (d) Grain diameter evolution

Figure 1. (A) Original 50xK DF TEM image showing the grain (in white contrast) of 50 K irradiated sample. (B) ML generated image showing the identified grains in yellow. (C) Comparison of the grain-size distribution at a fluence of around 7×10^{19} ions/m^2 using the M and ML methods. (D) Average grain diameter as a function of irradiation fluence. The errors are the standard deviation of measured grain diameters.

the heat is applied, and the length of time over which the heat source is maintained or the hold time. The values for these quantities were set to mimic the ion irradiation conditions used in the *in situ* experiments.

In this coupled model, the impact of irradiation is added via temperature changes due to thermal spikes. The thermal spikes cause the local temperature to increase, increasing the grain boundary mobility. This results in local grain boundary migration. The grain growth and heat-conduction models were fully coupled and solved simultaneously using an implicit finite element approach in MARMOT.

Results

Experimental Results

The major measurement in this project is the average grain diameter, determined by manual (M) and machine-learning (ML) methods. The M measurements were performed on both dark-field (DF) and bright-field (BF) TEM images at different magnifications to improve the statistics. ML measurements were only performed on 50 kX DF TEM images. Figure 1 compares the

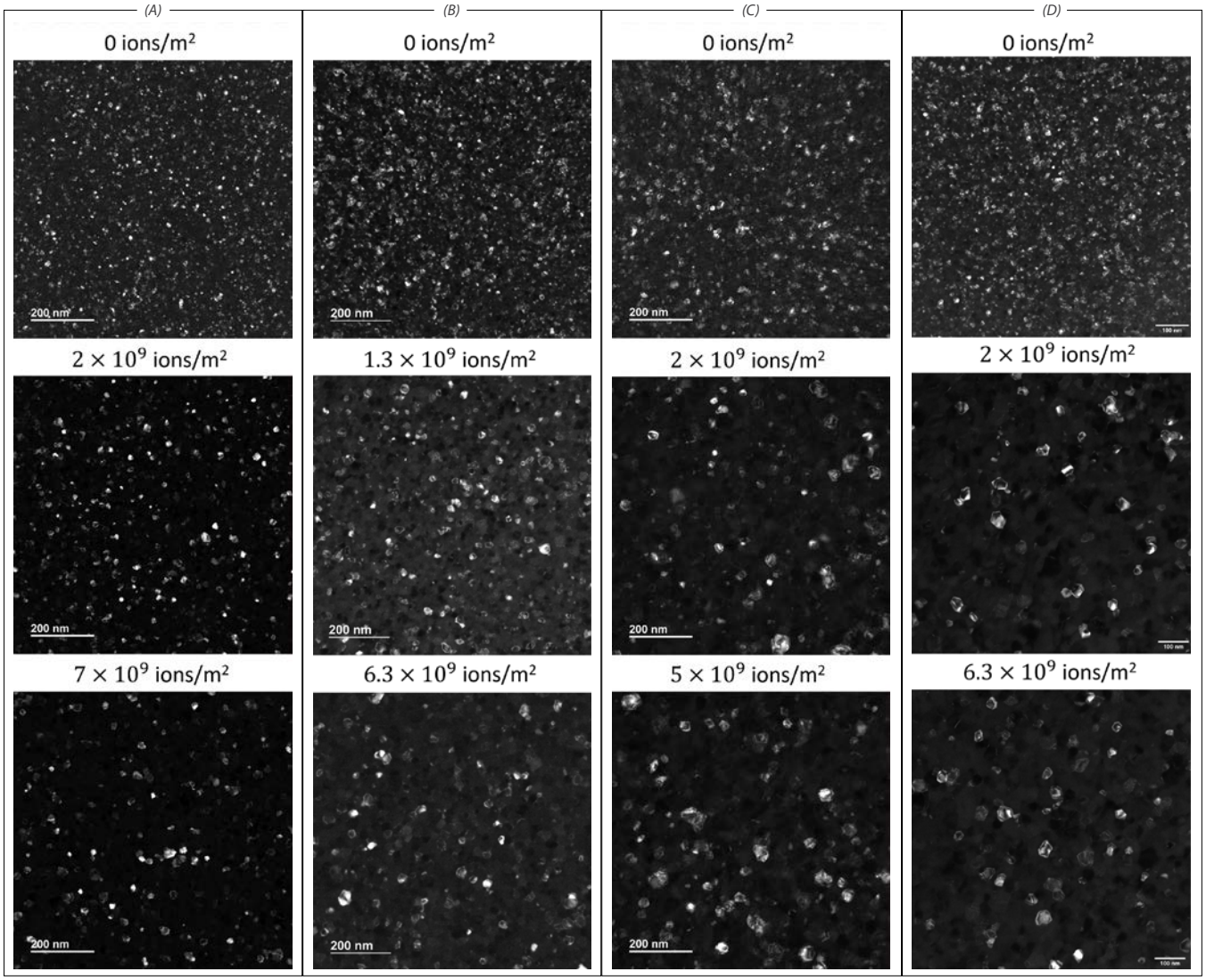

Figure 2. 50-xK DF TEM images showing the grain growth at (A) 50 K, (B) 475 K, (C) 675 K, and (D) 1075 K irradiation temperature up to 7×10^9 ions/m^2.

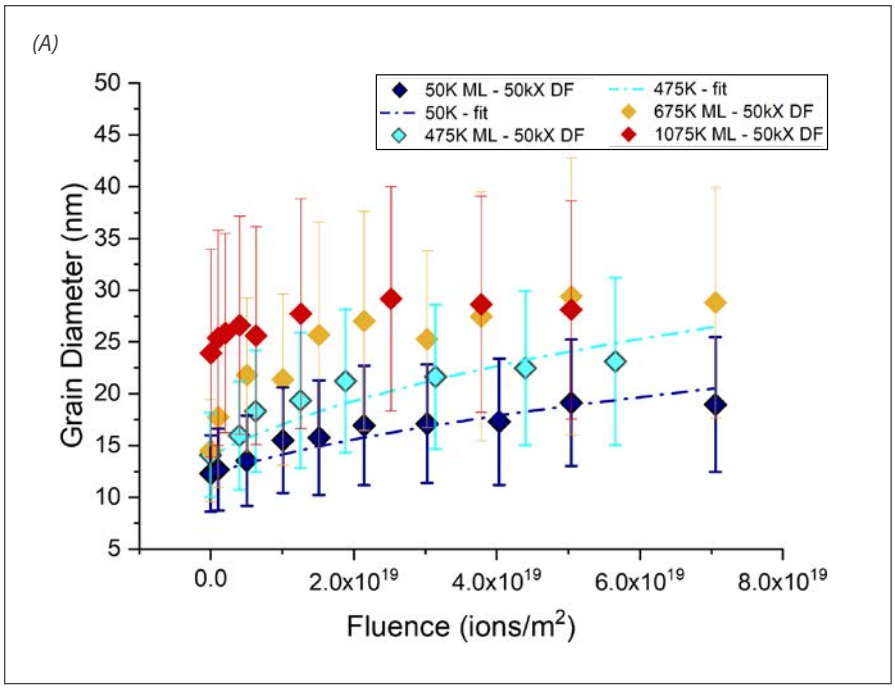

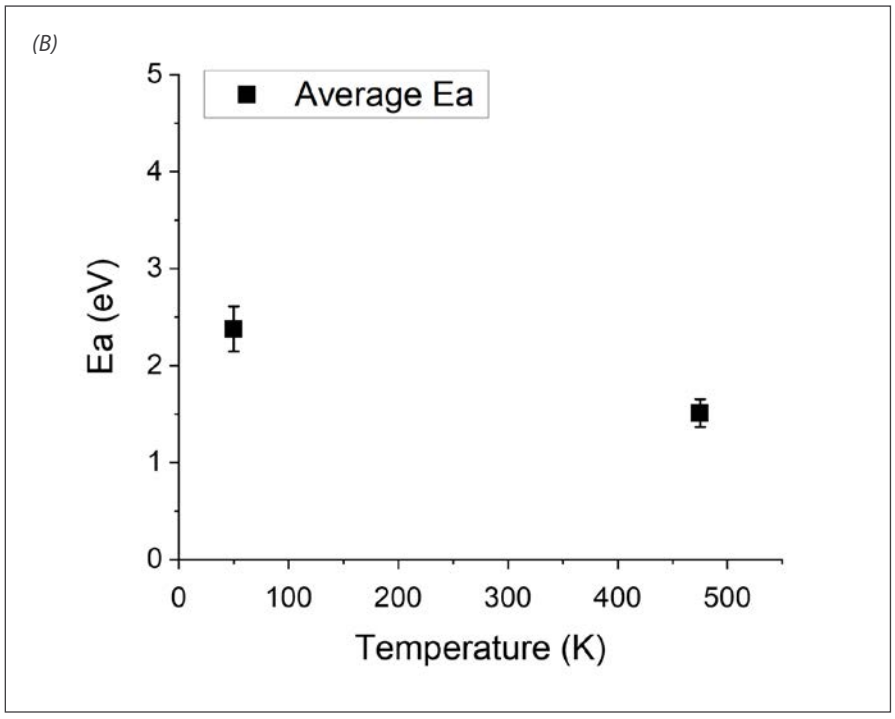

Figure 3. (A) Grain diameter evolution plot as a function of irradiation fluence at different irradiation temperatures. The errors are the standard deviation of measured grain diameters. (B) Calculated activation energy (E_a) for grain growth at 50 K and 475 K, respectively.

grain diameters measured by M and ML methods, respectively. The two methods show great consistency. The grain diameter evolution as a function of irradiation fluence at 50 K is also plotted in Figure 1 D. There is clear grain growth at 50 K under irradiation. Thermally driven grain growth would not occur at this temperature; therefore, the grain growth observed is purely an irradiation effect.

In addition to the 50 K irradiation experiments, additional studies were performed on UO_2 samples at higher temperatures. Figure 2 shows TEM images of sample irradiated at different temperatures. Qualitatively, the grain diameters appear to become much larger at higher doses for all temperatures. The grain diameters at higher irradiation temperature at 675 K and 1075 K are much larger than lower irradiation temperatures at 50 K and 475K.

A quantitative analysis on the grain growth kinetics was carried out, and the results are shown in Figure 3 (A). The grain growth at 675 K and 1075 K results from a combination of irradiation and thermally assisted processes; therefore, these grain growths were not analyzed. The data at 50 K and 475 K were fitted to a grain growth equation based on the thermal spike model [3].

The fitting equations are as follows:

(1)
$$D^3 - D_0^3 = K\phi t$$

(2)
$$K = \frac{36\gamma d_{spike} X \delta V_{at^v} \sqrt{\frac{3}{5}} \Gamma(\frac{8}{3}) k_B^{\frac{5}{3}}}{10\pi C_0^{\frac{2}{3}} k_0} \frac{Q^{\frac{5}{3}}}{(E_a^{spike})^{\frac{8}{3}}}$$

where D_0 is the initial grain diameter, ϕ is the ion flux (ions/m^2/s), t is time (s), and K is the growth rate (nm^3/[ions/m^2]), which is obtained by fitting Eq. (1) to the measured grain diameters. Other variables are described in Table 1. From Eq. (2), E_a can be calculated and is shown in Figure 3 (B) for two different temperatures. At 50 K, the E_a is about 2.5 eV, whereas it is about 1.5 eV at 475 K. However, E_a should be a temperature independent parameter. If data at 675 K and 1075 K were fitted to Eqs. (1) and (2), the calculated E_a would be even smaller. This is because Eq. (2) is only valid for low temperature irradiation,

where there is no thermally assisted grain growth.

To evaluate the thermal effect on the grain growth, isothermal annealing experiments without irradiation were also performed. Both M and ML results are plotted in Figure 4. Only the annealing temperature higher than 475 K resulted in grain growth and grain growth started to plateau after about 2 hours. These data are fitted to two different thermal grain growth equations as following:

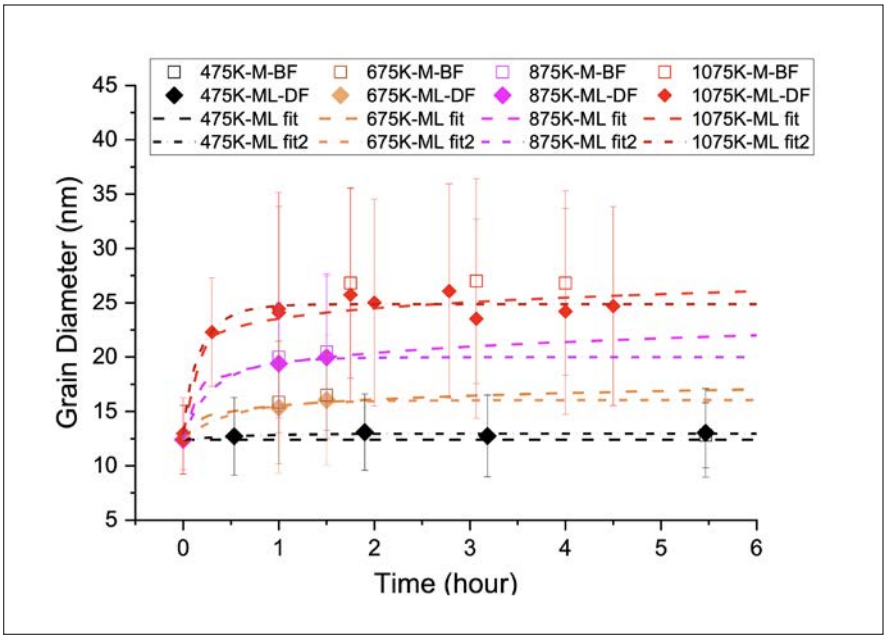

Figure 4. Grain diameter evolution under isothermal annealing.

(3) $$D^n - D_0^n = Mt$$

(4) $$\frac{dD}{dt} = A\left(\frac{1}{D} - \frac{1}{D_{max}}\right)$$

where D is the measured average grain diameter, D_0 is the initial average grain diameter, n is the growth rate exponent, M is a kinetic parameter, t is the annealing time, D_{max} is the measured maximum grain diameter, and A is another kinetic parameter similar to M. In Eq. (3), the values of n and M are fit to the data and in Eq. (4), the values of A and D_{max} are fit. For Eq. (3), n has to be greater than 10 to capture the plateau region, which is very high compared to other UO_2 data. Eq. 4

Parameters	Variables	Values
Average grain boundary energy	γ	1 (J/m^2)
Thermal spike diameter	d_{spike}	9.63 (nm)
Thermal spikes per ion	X	0.0407 (spikes/ion/nm)
Grain boundary width	δ	0.6 (nm)
Atomic volume	V_{at}	0.0136 (nm^3/atm)
Debye frequency	v	2.20 (THz)
Boltzmann constant	k_B	8.62×10^{-5} (eV/K)
Average thermal spike energy	Q	25.27 keV
Heat capacity	C_0	213.96 (J/mol/K)
Thermal conductivity	k_0	3 (W/m K)

Table 1. The description and literature values of the variables needed to calculate the thermal spike grain growth kinetic parameter K [6-31].

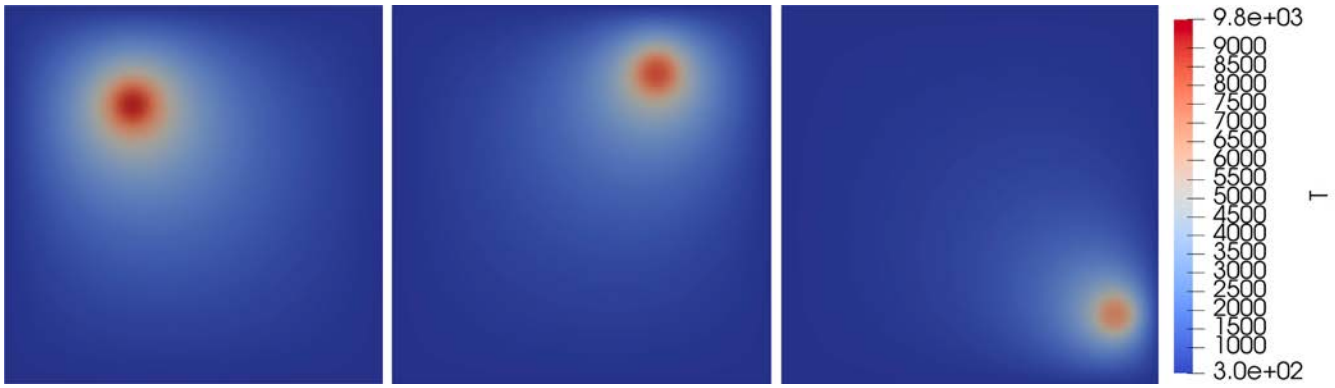

Figure 5. Simulation results with just heat conduction, where thermal spikes occur at random times and locations within the 300 × 300 nm domain. The temperature profile is shown after three different random spike events.

captures the plateau region well. By using a parameter described in [10] to obtain the A parameter, the activation energy (Q) for thermal grain growth is calculated to be 2.45 eV, which is consistent to our previously calculated E_a based on the thermal spike model and is similar to what has been found for other UO_2 grain growth data [1].

MARMOT Model Results

To test the behavior of thermal spikes in the heat conduction model, it was run separately from the grain growth model. A 30 × 30 nm 2D domain of UO_2 was simulated during irradiation with 1 MeV Kr ions at 300 K. The temperature at the domain boundaries was fixed at 300 K to represent the heat sink around the sample. The temperature profile after various thermal spikes is shown in Figure 5. The temperature gets very large within the thermal spike, reaching nearly 10,000 K. However, after the thermal spike, the heat quickly dissipates throughout the domain and the domain returns to 300 K. The temperature is higher in thermal spikes further from the boundaries then in spikes that are near the boundaries.

Grain growth at 300 K was then modeled in a 30 × 30 nm 2D domain with and without ion irradiation. A grain structure was generated with an average grain size of 4 nm, shown in Figure 6(a), similar to the average grain size in the UO_2 thin films used in the ion irradiation experiments. Grain growth was modeled for 5000 s. Without irradiation, the final microstructure, shown in Figure 6(b), was identical to the initial grain structure. This is consistent with the thermal grain growth experiments, in which grain growth did not occur in temperatures below 475 K. With irradiation, the coupled grain growth and heat-conduction model that included

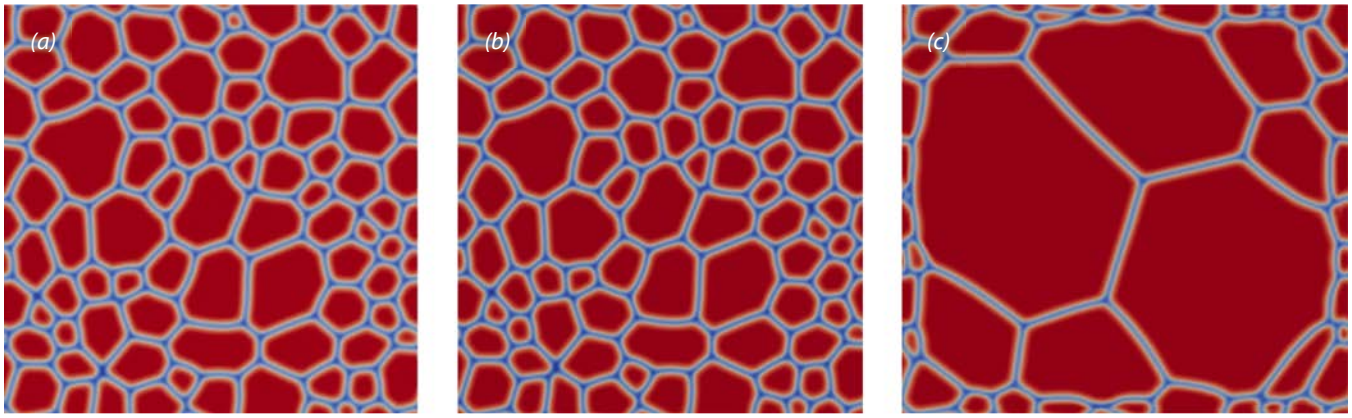

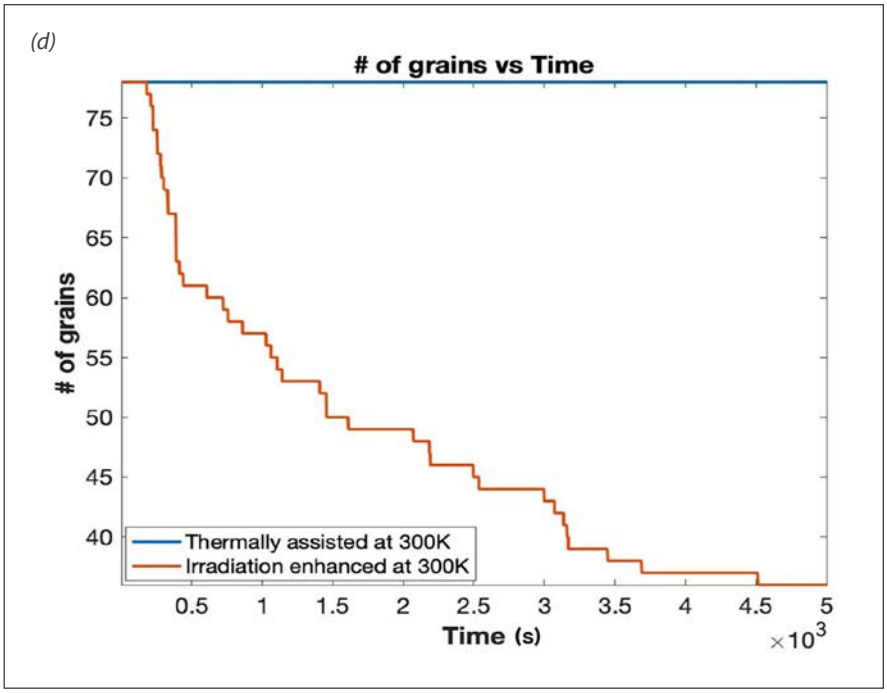

Figure 6. Comparison of grain growth with and without ion irradiation simulated using MARMOT in a 300 × 300 nm domain at 300 K. (a) The initial grain structure; (b) and (c) the grain structure after 5000 s without and with irradiation, respectively. (d) The number of grains versus simulation time. In (a–c), grains are shown in red and grain boundaries in blue.

the thermal spikes predicted a large amount of grain growth as shown in Figure 6(c). The grains grew quickly away from the boundaries; however, near the boundaries, much less grain growth occurred due to the fixed 300 K temperature at the boundaries. The number of grains went from 77 in the initial structure to 46 after 5000 s, as shown in Figure 6(d).

Discussion

This work builds directly on work that is already completed or underway for the NEAMS program. The current status and data needs of MARMOT align well with this research. *In situ* TEM characterization has provided initial and final

microstructures, per grain size and well controlled experimental conditions that are all desirable for MARMOT validation data. In particular, the grain growth data of nanocrystalline samples is desired, including both "annealing of well characterized microstructures" and "grain growth under irradiation," both of which have been achieved with the *in situ* TEM experiment. This work has also enhanced the capabilities of MARMOT, adding the impact of thermal spikes on grain growth. The new data will be used to validate the new MARMOT capability. While the design of this *in situ* experiment requires conditions atypical of those in reactor, the underlying science is the same and advancements made with these experiments are applicable to in reactor conditions. In fact, once the model in MARMOT has been fully developed and validated, it will be used to assess the impact of irradiation on UO_2 grain microstructure at light water reactor (LWR) conditions and if this effect should be included in the BISON fuel performance tool.

Conclusion

The impact of irradiation on grain growth in UO_2 was investigated using ion irradiation. This effect was also added to the MARMOT tool. Grain growth under irradiation occurred even at 50 K; higher irradiation temperatures led to gradually increasing grain growth rates. The calculated activation energy (E_a) for irradiation induced grain growth based on the thermal spike model was about 2.5 eV. The isothermal annealing results show the grains only start to grow at temperature higher than 475 K. The calculated thermal activation energy (Q) based on classical thermal grain growth equation with extra resistive force provide a similar activation energy. At temperature greater than 475 K in irradiated samples, grain growth occurred due to both thermal and irradiation-enhanced grain growth. The MARMOT UO_2 grain growth model was coupled to a heat-conduction model, including thermal spikes, and the resultant model predicted no thermal grain growth at 300 K but significant irradiation enhanced grain growth.

Future Activities

The primary remaining goal for this project is to validate the irradiation enhanced grain growth model in MARMOT. The temperatures and irradiation conditions used in the *in situ* experiments will be duplicated in grain growth simulations with many more grains and for longer times than the simulation shown in Figure 6. The results from the model will be direclty compared with the data and the model accuracy will be assessed. The validated MARMOT model will then be used to determine if irradiation enhanced grain growth needs to be included in the BISON grain growth model.

References

[1.] M. R. Tonks, P. C. A. Simon, J. Hirschhorn. "Mechanistic grain growth model for fresh and irradiated UO_2 nuclear fuel." *J. Nucl. Mater.* 543 (2021) 152576. https://doi.org/10.1016/j.jnucmat.2020.152576.

[2.] R. T. Michael, Z. Yongfeng, B. Aaron, B. Xian-Ming. "Development of a grain boundary pinning model that considers particle size distribution using the phase field method." *Model. Simul. Mater. Sci. Eng.* 23 (2015) 45009. http://stacks.iop.org/0965-0393/23/i=4/a=045009.

[3.] D. Kaoumi, A. T. Motta, R. C. Birtcher. "A thermal spike model of grain growth under irradiation." *J. Appl. Phys.* 104 (2008) 1–13. https://doi.org/10.1063/1.2988142.

[4.] W. Voegeli, K. Albe, H. Hahn. "Simulation of grain growth in nanocrystalline nickel induced by ion irradiation." *Nucl. Instruments Methods Phys. Res. Sect. B Beam Interact. with Mater. Atoms.* 202 (2003) 230–235. https://doi.org/10.1016/S0168-583X(02)01862-1.

[5.] O. Ronneberger, P. Fischer, T. Brox. "U-net: Convolutional networks for biomedical image segmentation." *Lect. Notes Comput. Sci.* (Including Subser. Lect. Notes Artif. Intell. Lect. Notes Bioinformatics). 9351 (2015) 234–241. https://doi.org/10.1007/978-3-319-24574-4_28.

[6.] P. S. Maiya. "Surface diffusion, surface free energy, and grain-boundary free energy of uranium dioxide." *J. Nucl. Mater.* 40 (1971) 57–65. https://doi.org/10.1016/0022-3115(71)90116-4.

[7.] E. N. Hodkin, M. G. Nicholas. "Surface and interfacial properties of non-stoichiometric uranium dioxide." *J. Nucl. Mater.* 67 (1977) 171–180. https://doi.org/10.1016/0022-3115(77)90172-6.

[8.] P. Nikolopoulos, S. Nazaré, F. Thümmler. "Surface, grain boundary and interfacial energies in UO_2 and UO_2-Ni." *J. Nucl. Mater.* 71 (1977) 89–94. https://doi.org/10.1016/0022-3115(77)90191-X.

[9.] P. V. Nerikar, K. Rudman, T.G. Desai, D. Byler, C. Unal, K. J. McClellan, S. R. Phillpot, S. B. Sinnott, P. Peralta, B. P. Uberuaga, C. R. Stanek. "Grain boundaries in uranium dioxide: Scanning electron microscopy experiments and atomistic simulations." *J. Am. Ceram. Soc.* 94 (2011) 1893–1900. https://doi.org/10.1111/j.1551-2916.2010.04295.x.

[10.] Y. Zhang, P. C. Millett, M. R. Tonks, X. M. Bai, S. B. Biner. "Molecular dynamics simulations of intergranular fracture in UO_2 with nine empirical interatomic potentials." *J. Nucl. Mater.* 452 (2014) 296–303. https://doi.org/10.1016/j.jnucmat.2014.05.034.

[11.] E. Bourasseau, A. Mouret, P. Fantou, X. Iltis, R.C. Belin, Experimental and simulation study of grain boundaries in UO_2, *J. Nucl. Mater.* 517 (2019) 286–295. https://doi.org/10.1016/j.jnucmat.2019.02.033.

[12.] A. Ksibi, E. Bourasseau, X. Iltis, D. Drouan, M. Gaudet, A. Germain, A. Pena, G. Lapertot, J. P. Brison, R. C. Belin, "Experimental and numerical assessment of grain boundary energies in polycrystalline uranium dioxide." *J. Eur. Ceram. Soc.* 40 (2020) 4191–4201. https://doi.org/10.1016/j.jeurceramsoc.2020.04.041

[13.] C.J . Ulmer, W. Y. Chen, D. E. Wolfe, A. T. Motta. "*In-situ* ion irradiation induced grain growth in nanocrystalline ceria." *J. Nucl. Mater.* 545 (2021) 152688. https://doi.org/10.1016/j.jnucmat.2020.152688.

[14.] T. G. Godfrey, W. Fulkerson, T. G. Kollie, J .P. Moore, D. L. McElroy. "Thermal Conductivity of Uranium Dioxide from

-57° to 1100°C by a Radial Heat Flow Technique." *J. Am. Ceram. Soc.* 48 (1965) 297–305. https://doi.org/10.1111/j.1151-2916.1965.tb14745.x.

[15.] T. K. Engel, The heat capacities of Al_2O_3, UO_2 and PuO_2 From 300 To 1100 °K, *J. Nucl. Mater.* 31 (1969) 211–214. https://doi.org/10.1016/0022-3115(69)90194-9.

[16.] F. Grønvold, N. J. Kveseth, A. Sveen, J. Tichý. "Thermodynamics of the UO_{2+x} phase I. Heat capacities of $UO_{2.017}$ and $UO_{2.254}$ from 300 to 1000 K and electronic contributions." *J. Chem. Thermodyn.* 2 (1970) 665–679. https://doi.org/10.1016/0021-9614(70)90042-X.

[17.] J. J. Huntzicker, E. F. Westrum. "The magnetic transition, heat capacity, and thermodynamic properties of uranium dioxide from 5 to 350 K." *J. Chem. Thermodyn.* 3 (1971) 61–76. https://doi.org/10.1016/S0021-9614(71)80067-8.

[18.] H. Inaba, K. Naito, M. Oguma. "Heat capacity measurement of $U_{1-y}Gd_yO_2$ ($0.00 \leqq y \leqq 0.142$) from 310 to 1500 K." *J. Nucl. Mater.* 149 (1987) 341–348. https://doi.org/10.1016/0022-3115(87)90536-8.

[19.] Y. Takahashi, M. Asou. "High-temperature heat-capacity measurements on (U, Gd)O_2 by drop calorimetry and DSC." *J. Nucl. Mater.* 201 (1993) 108–114. https://doi.org/10.1016/0022-3115(93)90164-T.

[20.] C. Ronchi, M. Sheindlin, M. Musella, G. J. Hyland. "Thermal conductivity of uranium dioxide up to 2900 K from simultaneous measurement of the heat capacity and thermal diffusivity." *J. Appl. Phys.* 85 (1999) 776–789. https://doi.org/10.1063/1.369159.

[21.] P. Goel, N. Choudhury, S. L. Chaplot. "Atomistic modeling of the vibrational and thermodynamic properties of uranium dioxide, UO_2." *J. Nucl. Mater.* 377 (2008) 438–443. https://doi.org/10.1016/j.jnucmat.2008.03.020.

[22.] Y. Yun, D. Legut, P. M. Oppeneer. "Phonon spectrum, thermal expansion and heat capacity of UO_2 from first-principles." *J. Nucl. Mater.* 426 (2012) 109–114. https://doi.org/10.1016/j.jnucmat.2012.03.017.

[23.] J. K. Fink. "Thermophysical properties of uranium dioxide." *J. Nucl. Mater.* 279 (2000) 1–18. https://doi.org/10.1016/S0022-3115(99)00273-1.

[24.] B. T. Wang, J. J. Zheng, X. Qu, W. D. Li, P. Zhang. "Thermal conductivity of UO_2 and PuO_2 from first-principles." *J. Alloys Compd.* 628 (2015) 267–271. https://doi.org/10.1016/j.jallcom.2014.12.204.

[25.] W. D. Kingery, J. Francl, R. L. Coble, T. Vasilos. "Thermal Conductivity: X, Data for Several Pure Oxide Materials Corrected to Zero Porosity." *J. Am. Ceram. Soc.* 37 (1954)

107–110. https://doi.org/10.1111/j.1551-2916.1954.tb20109.x.

[26.] M. Sheindlin, D. Staicu, C. Ronchi, L. Game-Arnaud, B. Remy, A. Degiovanni. "Experimental determination of the thermal conductivity of liquid UO_2 near the melting point." *J. Appl. Phys.* 101 (2007). https://doi.org/10.1063/1.2721091.

[27.] V. G. Baranov, Y. N. Devyatko, A. V. Tenishev, A. V. Khlunov, O. V. Khomyakov. "New method for determining the temperature dependence of the thermal conductivity coefficient of dielectrics in a pulse experiment." *Inorg. Mater. Appl. Res.* 1 (2010) 167–173. https://doi.org/10.1134/S2075113310020164.

[28.] R. L. Gibby. "The effect of plutonium content on the thermal conductivity of (U, Pu)O_2 solid solutions." *J. Nucl. Mater.* 38 (1971) 163–177. https://doi.org/10.1016/0022-3115(71)90040-7.

[29.] J. L. Bates. *High-temperature Thermal Conductivity of "Round Robin" Uranium Dioxide.* BNWL-1431. Brookhaven National Laboratory. 1970.

[30.] J. W. L. Pang, W. J. L. Buyers, A. Chernatynskiy, M. D. Lumsden, B. C. Larson, S. R. Phillpot. "Phonon lifetime investigation of anharmonicity and thermal conductivity of UO_2 by neutron scattering and theory." *Phys. Rev. Lett.* 110 (2013) 1–5. https://doi.org/10.1103/PhysRevLet.110.157401.

[31.] H. Kim, M.H. Kim, M. Kaviany, Lattice thermal conductivity of UO_2 using ab-initio and classical molecular dynamics, J. Appl. Phys. 115 (2014). https://doi.org/10.1063/1.4869669.

Distributed Partnership at a Glance

NSUF Institution	Facilities and Capabilities
Argonne National Laboratory	The Intermediate Voltage Electron Microscopy – Tandem Facility
Collaborators	
Argonne National Laboratory	Memei Li (collaborator), Wei-Ying Chen (collaborator)
Los Alamos National Laboratory	Aiping Chen (collaborator)
Penn State University	Zefeng Yu (co-principal investigator)
University of Florida	Ali Muntaha (collaborator), Michael Tonks (co-principal investigator)